Available online at www.sciencedirect.com
SCIENCE DIRECT®
Surface & Coatings Technology xx (2005) xxx–xxx
SURFACE & COATINGS TECHNOLOGY
www.elsevier.com/locate/surfcoat

Tribocorrosion behaviour of ZrO_xN_y thin films for decorative applications

S.C. Ferreira [a], E. Ariza [a], L.A. Rocha [a,*], J.R. Gomes [a], P. Carvalho [b], F. Vaz [b], A.C. Fernandes [b], L. Rebouta [b], L. Cunha [b], E. Alves [c], Ph. Goudeau [d], J.P. Rivière [d]

[a] *Universidade do Minho, Dept. Eng. Mecânica, Azurém, 4800-058 Guimarães, Portugal*
[b] *Universidade do Minho, Dept. Física, Azurém, 4800-058 Guimarães, Portugal*
[c] *ITN, Departamento de Física, E.N.10, 2685 Sacavém, Portugal*
[d] *Laboratoire de Métallurgie Physique, Université de Poitiers, 86960 Futuroscope, France*

Abstract

The aim of this work is the investigation of the tribocorrosion behaviour of single layered zirconium oxynitride, ZrO_xN_y, thin films in reciprocating sliding and immersed in an artificial sweat solution at room temperature. During the wear tests samples were kept under potentiostatic control and the corrosion current were monitored. Also, Electrochemical Impedance Spectroscopy (EIS) tests were performed before and after sliding in order to evaluate, in detail, the modification of the protective character of the coating caused by the joint action of wear and corrosion. The modifications of the coating structure and microstructure and/or chemical composition originated by the variation of the deposition parameters were also evaluated and correlated with the corrosion mechanisms occurring in each system.

Keywords: Tribocorrosion; Decorative films; Zirconium; EIS

1. Introduction

Vacuum coating techniques, especially Physical Vapour Deposition (PVD) of decorative layers has been industrially used for more than 15 years. Decorative hard coatings have first been introduced on small decorative parts such as watches, writing instruments and spectacles frames. In the last few years, there has been considerable interest in the production of metallic oxynitride thin films, MeO_xN_y (Me = early transition metal) [1–6], since the presence of oxygen in nitride compounds leads to unexpected and promising functional range of materials. The presence of oxygen allows the tailoring of film properties between those of metallic nitrides, MN_y, and those of the correspondent insulating oxides, MO_x. Tuning the metallic/covalent and ionic bonding characteristics allows one to tune the mechanical, electrical, chemical and optical properties of materials, including colour. Recent publications suggest that the performance of these oxynitrides depends not only on the deposition method but also on both the concentration and distribution of the nitrogen atoms incorporated into the matrix [1–9].

Decorative thin films may be exposed to aggressive chemical environments, such as human sweat, while, at the same time, they can also be subjected to wear due to hand touch or cleaning procedures. The degradation of the materials by mechanical (wear), chemical and electrochemical processes is defined as tribocorrosion [10–13]. The interactions of chemical and mechanical parameters on the tribocorrosion behaviour cannot be always predicted on the basis of separate wear and corrosion experiments. In fact, wear accelerated corrosion arises from the fact that an asperity rubbing on a surface produces a clean track which is usually more sensitive to corrosion than the same surface in the absence of rubbing conditions, thus contributing to removal of material [14,15]. Also, the presence of pores in the film, among other chemical, electrochemical, physical and mechanical factors, can lead to the attack of the substrate contributing to the material degradation in the tribological contact [16,17]. Many aspects of the tribocorrosion mechanisms acting on thin films are not yet fully understood, partly due to the complexity of the processes involved.

The main purpose of this work consists on the study of the corrosion behaviour and degradation mechanisms of decorative

* Corresponding author. Tel.: +351 253 510 231; fax: +351 253 516 007.
E-mail address: lrocha@dem.uminho.pt (L.A. Rocha).

0257-8972/$ - see front matter © 2005 Elsevier B.V. All rights reserved.
doi:10.1016/j.surfcoat.2005.11.083

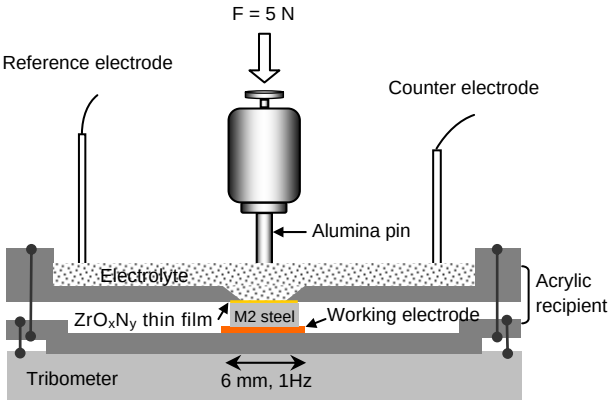

Fig. 1. Schematic view of tribometer and electrochemical cell used in the tribocorrosion tests.

ZrO_xN_y thin films, when they are under the simultaneous action of mechanical (wear) and chemical aggressive environments (artificial sweat solution), i.e., tribocorrosion. Special attention is given to the study of effect of modifications in microstructure and/or chemical composition induced by the variation of the deposition parameters of thin films (flow of reactive gases, oxygen/nitrogen ratio) on the tribocorrosion process.

2. Experimental details

ZrO_xN_y thin films were deposited onto high-speed steel (AISI M2) by reactive dc magnetron sputtering in a laboratory-size deposition system [18]. The films were prepared with the substrate holder positioned at 70 mm from the zirconium target in all runs, using a dc power supply with a density of 100 A m^{-2} on the target (99.6 at.% purity). A gas atmosphere composed of argon (working gas) and a reactive mixture composed of nitrogen + oxygen (19 : 1 ratio) was used. The working gas flow was kept constant at 55 sccm and the reactive gas flow varied from 5.5 to 16 sccm. The working pressure was kept approximately constant at 0.4 Pa and the substrates were grounded.

The atomic composition of the as deposited samp1es was measured by Rutherford Backscattering Spectroscopy (RBS) using a 2 MeV He^+ beam. Ball cratering tests were used to measure the thickness of the films. In order to examine the film structure, X ray diffraction experiments (XRD) were undertaken in a Philips PW 1710 apparatus, using Cu Kα radiation. Surface and cross-section morphological features of the films were studied by Scanning Electron Microscopy (SEM) and Atomic Force Microscopy (AFM). Analysis by Optical Microscopy (OM) was also used in order to quantify film's surface defects — area and density.

Potentiodynamic polarisation tests, in both the ZrO_xN_y films and on the M2 steel substrate were performed between −800 mV to 2000 mV at a scan rate of 2 mV s^{-1} using a PGP201 Potentiostat/Galvanostat (Radiometer Analytical, Denmark), controlled by the VoltaMaster-1 software.

The tribocorrosion tests were performed using a reciprocating tribometer (Plint TE67/R). An alumina pin (truncated cone geometry and with a tip of 1 mm in diameter) was used as counterbody and mounted vertically on the samples immersed in the electrolyte (exposed area = 0.95 cm^2). The ZrO_xN_y films were used as plates positioned horizontally and mounted in an acrylic electrochemical cell (20 ml electrolyte volume) with the working surface of the film facing upwards (see Fig. 1). An artificial sweat solution (pH = 4.5), containing 7.5 g l^{-1} NaCl; 1.2 g l^{-1} KCl; 1 g l^{-1} CH_4N_2O (urea) and 1 g l^{-1} $C_3H_6O_3$ (lactic acid), was used as electrolyte. All potentials are measured and expressed with reference to a standard calomel electrode (SCE), and a platinum wire with an area of 1 cm^2 served as counter electrode. A Voltalab PGZ100 Potentiostat (Radiometer Analytical, Denmark), controlled by Voltamaster-4 Software was used in for potentiostatic control and for performing the EIS experiments.

Samples were previously cathodically polarised at −900 mV vs. SCE, during 3 min. Subsequently, a potential of −660 mV vs. SCE was applied to stabilise the samples by a period of 10 min. Then, electrochemical impedance spectroscopy (EIS) measurements were performed in the frequency range from 100 kHz to 15.823 mHz, with an AC sine wave amplitude of 10 mV applied to the electrode, keeping the sample under potentiostatic control (at E_{corr} of the steel, i.e., in the catholic region of the films).

Next, the mechanical contact between the alumina pin and the ZrO_xN_y plate was established. The reciprocating wear test was performed with a normal load of 5 N, displacement amplitude of 6 mm and a frequency of 1 Hz. The sliding time was 3600 s corresponding approximately to 3667 strokes. When sliding was stopped, the pin was removed, and another EIS measurement was performed. At the end of the test the plate and the pin were removed from the solution and cleaned ultrasonically in ethanol. For each sample the tests were repeated twice. The wear volume was determined by a profilometer method, using a Perthometer S5P roughness meter, by calculating the average cross-sectional area multiplied by the stroke length.

3. Results and discussion

3.1. Structural and morphological characterization

A summary of the samples analyzed in this work is illustrated in Table 1. RUMP composition simulations [19] revealed a homogeneous in-depth composition profile for all films [20].

Table 1
Composition, thickness, grain size and density of defects of studied samples

Flow (sccm)	Zr (at.%)	N (at.%)	O (at.%)	Thickness (μm)	Grain size (nm)	Density of defects (mm^{-2})
ZrN– (only N – 11)	50	50	–	5.2±0.2	11	96.51
5.5	48.6	48.2	3.1	6.2±0.1	10	73.16
9	44.9	46.8	7.9	4.1±0.1	11	125.18
12.5	40.8	45.7	13.1	3.8±0.3	3	78.86
16	41.1	45.5	13.2	3.2±0.3	3	81.07
ZrO_2– (only O – 12.5)	33.3	–	66.6	2.9±0.5	11	73.16

Fig. 2 shows the XRD diffraction patterns for the ZrO_xN_y samples. For the film prepared with a reactive gas flow of 5.5 sccm a B1-NaCl crystal structure is detected, which is typical for ZrN films. With the increase of the reactive gas flow, there is a change from a roughly random orientation (typical of the 5.5 sccm sample) to a preferential orientation <100>, clearly visible for the 9 sccm sample. This change in the preferential orientation is followed by some modification on the structure. It appears that at this gas flow, the films present an intermediate structure between that of ZrN, and of the oxygen doped Zr_3N_4 structure type, which seems to be already the dominant one in the film deposit with 12.5 sccm. For the film deposited with a reactive gas flow of 16 sccm (revealing the highest oxygen content), there is another structural change, but, the reduced number of visible diffraction peaks does not allow a detailed and conclusive analysis. Nevertheless, the diffraction peak at $2\theta \approx 31.3°$ could be assigned to the (111) planes of a zirconium oxide monoclinic-type structure, which in fact correlates with the "pure" zirconium oxide identified in the ZrO_2, sample. The possibility of having a zirconium oxide orthorhombic structure should also be considered, which would then result from the evolution of the oxygen-doped Zr_3N_4 phase towards an oxide type one (with possible nitrogen inclusions).

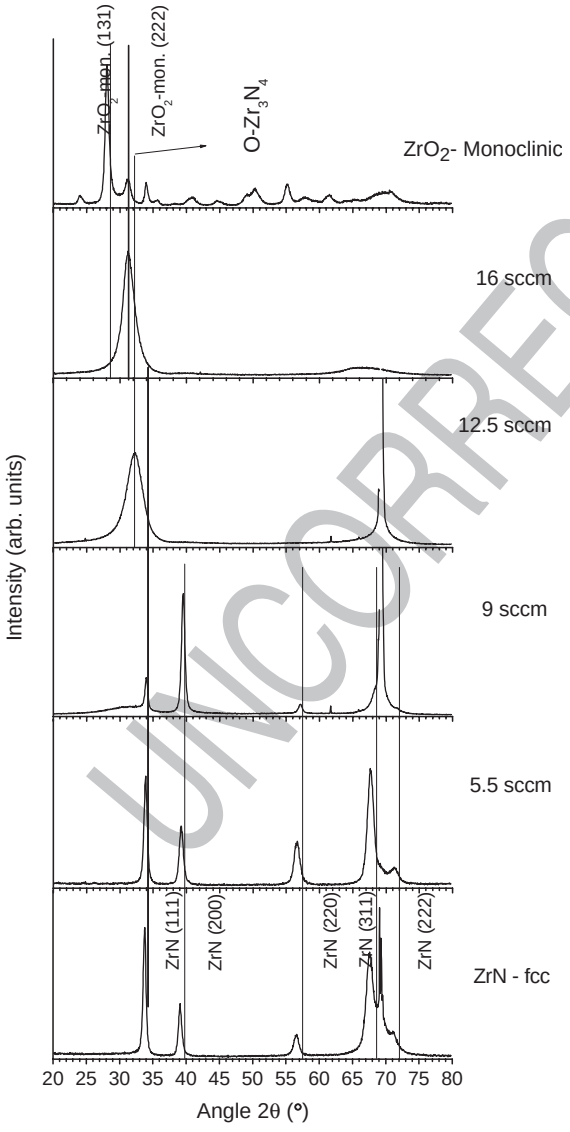

Fig. 2. XRD patterns for the different ZrO_xN_y films. The vertical lines indicate the diffraction peak position of the reference ZrN phase.

SEM cross-sections images of the zirconium nitride film revealed that these films grow with a columnar-type structure, lying in the transition between T and I zones of Thornton's zone model [21]. The process of surface diffusion is not very high (the samples were prepared with no ion bombardment) and the films are formed by narrow columnar grains with a densely packed fibrous morphology, with a superficial dome-rounded shape of the columnar grains [22]. With the increasing of the oxygen content, the films tend to develop a featureless structure, with a clear tendency for the densification of the microstructure. The evolution of the structure and the subsequent changes on the morphology of the films are well correlated with the AFM results (Fig. 3). In this figure, it is possible to observe that the sample deposited with low reactive gas flow (5.5 sccm) revealed the lowest roughness. Increasing the reactive gas flow (9 sccm), and the consequential increase of the oxygen content, a substantial increase of the coatings roughness is revealed. This evolution in roughness is probably the consequence of the already mentioned increase of coating disorder/defects, promoted by the possible inclusion of oxygen atoms in the ZrN lattice [4], and also the tendency to develop a structure between the fcc ZrN and a oxygen doped Zr_3N_4 orthorhombic phase. The sample deposited with 12.5 sccm, presents a decrease of the roughness, probably due to the formation of a poorly crystallized (tending to amorphization) oxygen-doped Zr_3N_4 type phase.

3.2. Electrochemical and tribocorrosion behaviour

3.2.1. Potentiodynamic polarisation tests

In Fig. 4 results obtained in potentiodynamic polarisation tests performed on the coated samples are plotted. For comparison, the curve obtained for the M2 steel is also presented. From the polarisation curves the corrosion current density was calculated and is referred in the graph. As it can be observed, the presence of the thin films clearly improves the corrosion properties of the M2 steel. A notorious enhancement of corrosion current density (i_{corr}) is observed for the ZrN film and for the ZrO_xN_y films. The ZrO_2 film, however, show a corrosion resistance slightly lower than the rest of the samples.

3.2.2. EIS measurements

Results obtained in the EIS measurements carried out before and after the sliding were fitted using an electrochemical equivalent circuit model composed by the electrolyte resistance and for two pairs of elements: the first composed by the capacitance and the polarisation resistance of the film (R_{pf}) and the second composed by the double layer capacitance and the polarisation resistance of the substrate (R_{ps}). The polarization resistance of the film (R_p) was then estimated by the sum of R_{ps} and R_{pf}, in accordance to the method described by Liu et al. [23]. Fig. 5 shows the polarisation resistance of the ZrN, ZrO_2

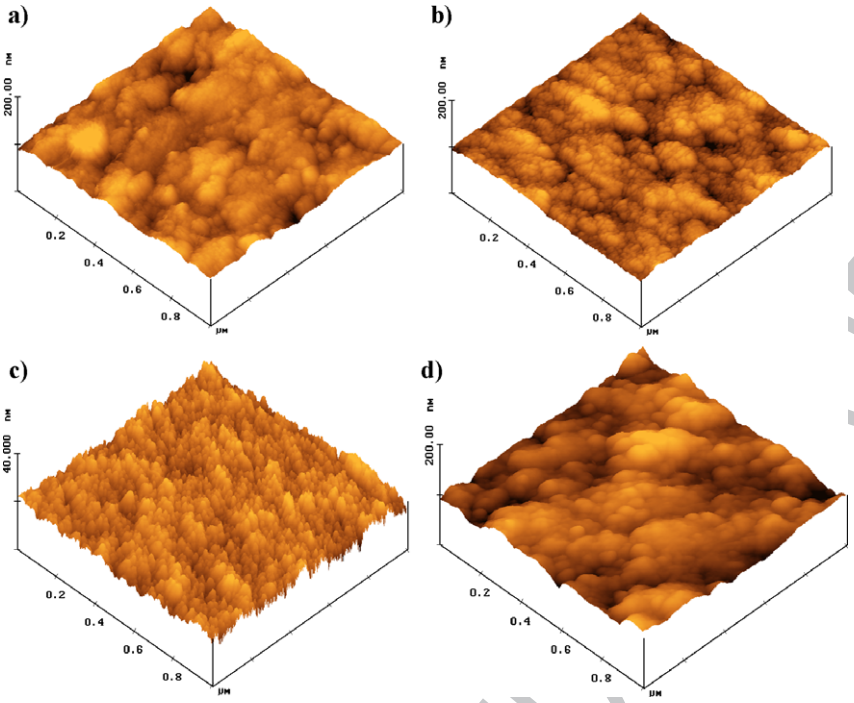

Fig. 3. Atomic Force Microscopy (AFM) images of: a) ZrN film; and of samples prepared with a reactive gas flow of: b) 5.5 sccm; c) 9 sccm; and d) 12.5 sccm.

and ZrO_xN_y films before and after sliding as a function of reactive gas flow. As it can be observed, R_p after sliding decreases in all films mainly due to mechanical damage. An important remark is that the ZrN film and the ZrO_xN_y film produced with a gas flow of 9 sccm, are those presenting the higher polarisation resistance when compared with the other films, this behaviour being in accordance with the i_{corr} values calculated from the potentiodynamic curves, as discussed above.

In order to obtain a better understanding of corrosion behaviour, a correlation between R_p and the film thickness was also plotted in Fig. 5. As it can be seen, an increase in the gas flow results in a decrease of the deposition rate, and thinner films are obtained (same deposition time). However, as it can be observed, there is no direct relation between the film thickness and the polarisation resistance, indicating that the corrosion behaviour of the samples is governed by a complex interaction of other parameters, such as microstructure and structure.

In Fig. 6 a correlation between R_p and the hardness of the films is presented. The hardness, being dependent on the structure of the films, is likely to contribute for the evaluation of the influence of the structural characteristics of the film on the corrosion behaviour. As it can be observed in the figure, a good correlation could be found between both parameters. Thus, the best corrosion resistance observed in the ZrO_xN_y film produced with a gas flow of 9 sccm, might be partially attributed to the fact that, as discussed above, this sample appears to be in a transition zone between the crystallographic structure of ZrN and an oxygen doped Zr_3N_4 type structure. Nevertheless, it

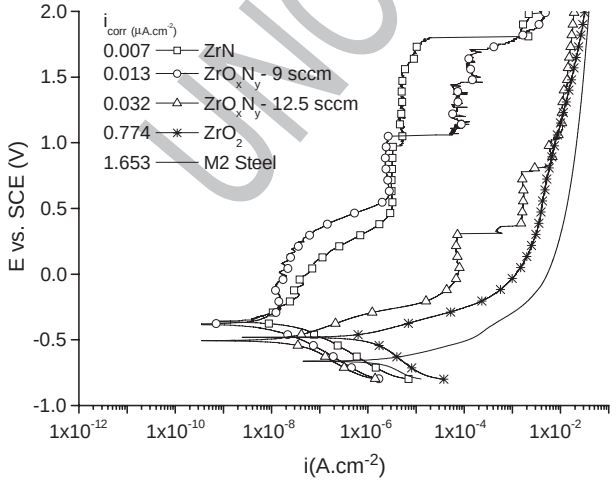

Fig. 4. Potentiodynamic polarisation curves obtained for ZrO_xN_y films immersed in artificial sweat solution.

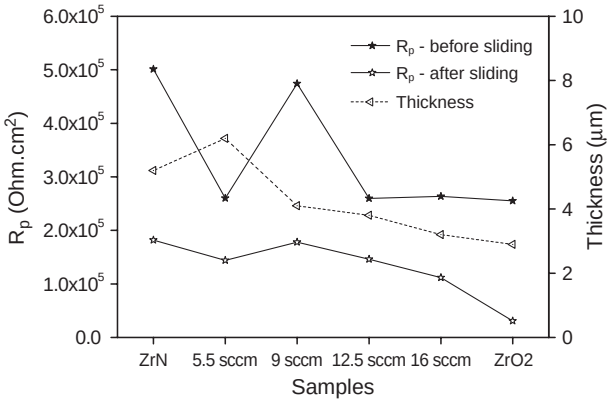

Fig. 5. Influence of the gas flow in the polarisation resistance and in the thickness of ZrO_xN_y films.

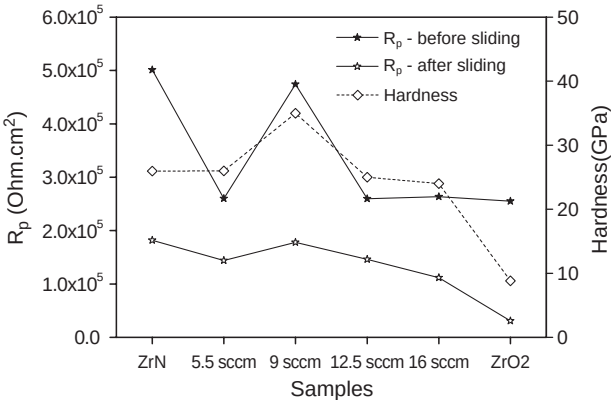

Fig. 6. Influence of the gas flow in the polarisation resistance and in the hardness of ZrO_xN_y films.

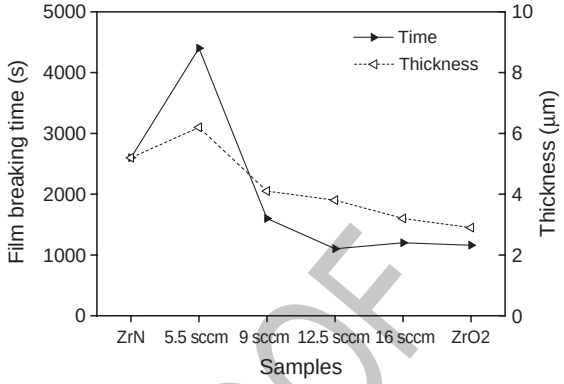

Fig. 8. Correlation between the film thickness and the film breaking time obtained in ZrO_xN_y films immersed in artificial sweat solution.

should be stressed that these are complex systems, and other structural aspects, related with the amount of defects, grain size, or degree of crystallinity of the films are expected to have some influence on this behaviour.

3.2.3. Tribocorrosion test

Fig. 7 shows the evolution of the corrosion current density and of the friction coefficient with the time, obtained in the ZrO_xN_y film obtained with a gas flow of 9 sccm. This curve is representative of the behaviour found in the other samples. As shown, at the beginning of sliding, the corrosion current density abruptly increases as a consequence of mechanical damage of the film. Also, as it can be observed, the friction coefficient follows the same trend as the corrosion current density during the entire wear test. As discussed by Ponthiaux et al. [10] and Mischler et al. [24], friction depends, in a complex way, from adhesion and deformation mechanisms which, in turn are directly related with surface chemistry. Thus, the friction coefficient is sensitive to the modifications occurring in the surface during the corrosion of the material. This behaviour was observed in all samples.

Both a high corrosion current density and a relatively high friction coefficient are maintained till a certain moment in which the films breaks and the alumina pin contacts directly the steel substrate, resulting in a rapid decrease of these two parameters. Then, both parameters remain relatively stable until the end of the sliding, with mean values similar to those found in a tribocorrosion test performed in the M2 steel without the presence of any film.

The time until the alumina pin directly contacts the substrate is related with the film thickness, as it can be observed in Fig. 8. In fact, under the tribological conditions used in this work (configuration of the pin and normal load) the destruction of the film appears to occur independently from other mechanical or topographical aspects such as hardness and/or roughness.

In the tribocorrosion tests, the total volume loss, originated by the synergistic contribution of the wear and corrosion was estimated. This parameter is shown in Fig. 9, as a function of the gas flow. Observing the graph, it is possible to see the strong correlation between the volume loss and the film thickness. As discussed above, the friction coefficient has a tendency to decrease down to similar values found in M2 steel, when the film is removed in the wear track region. Also, as shown in Fig. 7, both the friction coefficient and the corrosion current density are comparatively higher when the alumina pin is sliding on the films. Thus, apparently, most of the material removal arises from the destruction of the film. However, it should be kept in mind the strong influence of

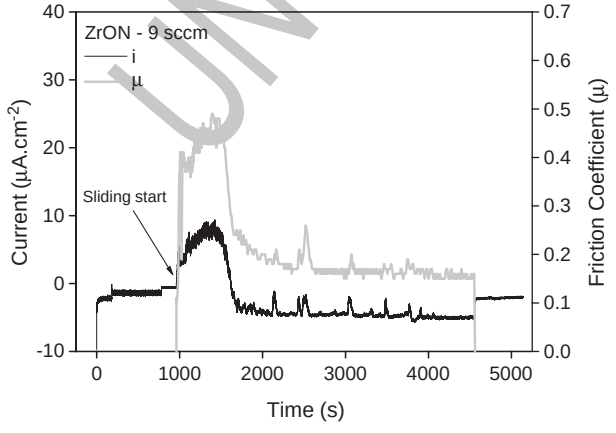

Fig. 7. Evolution of the corrosion current density and of the friction coefficient during the tribocorrosion tests.

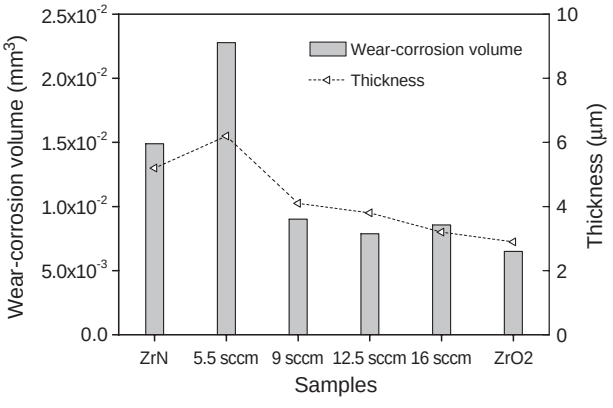

Fig. 9. Correlation between the volume loss caused by wear and corrosion with the thickness of ZrO_xN_y films immersed in artificial sweat solution.

the steel substrate in this behaviour. The tribocorrosion tests were performed with an applied potential of −660 mV vs. SCE, i.e, in the region of the E_{corr} of the steel substrate (see Fig. 4). In preliminary tests conducted with an applied potential of +750 mV vs. SCE, which lies on the passivation plateau of the coated samples, but in the active zone of the steel (see Fig. 4), it was observed that the film was destroyed even without being subjected to the wear action. The reason for this behaviour was the strong dissolution of the steel, caused by the applied potential, which caused the delamination of the film. Thus, the main contribution for the amount of material removed during sliding arises from the break and delamination of the film, but most probably, due to the dissolution of the steel underneath, which may be under crevice and/or galvanic coupling conditions while the film is present. The relatively high coefficient of friction observed during sliding, before the break of the film (see Fig. 7), might be attributed to the accumulation of corrosion products in the contact region and to the presence of particles from the film that are increasingly delaminated from the material.

4. Conclusions

In this work the tribocorrosion properties of ZrO_xN_y thin films in reciprocating sliding and immersed in an artificial sweat solution were evaluated.

It can be concluded that the deposited films clearly improve the corrosion properties of the M2 steel used as substrate. A notorious increase in the polarisation resistance of ZrO_xN_y film obtained with 9 sccm of gas flow was found. This behaviour was attributed to the fact that this sample is in the transition between the ZrN structure and an oxygen doped Zr_3N_4 type structure. The good corrosion behaviour present in the ZrN film is a product of the intrinsic good corrosion resistance of pure nitrides.

In tribocorrosion conditions under potentiostatic control the amount of material removed as well as the time needed for the film to be totally removed from the contact zone is related with the thickness of the film, i.e., with the amount of film present in the contact region. Although tests under potentiostatic control were conducted at the E_{corr} of the steel substrate, it is still the dissolution of the substrate that governs the degradation behaviour. In fact, under the potentiostatic conditions used in this work, the film is delaminated due to the preferential dissolution of the substrate.

Acknowledgements

The authors gratefully acknowledge the financial support of the European Union through the NMP3-CT-2003-505948 project “HARDECOAT”. Acknowledgments also to the Portuguese FCT institution by the contract SFRH/BPD/5518/2001 and by the project n° POCTI/CTM/38086/2001 co-financed by European community through FEDER.

References

[1] F. Vaz, P. Cerqueira, L. Rebouta, S.M.C. Nascimento, E. Alves, Ph. Goudeau, J.P. Rivière, Surf. Coat. Technol. 174–175 (2003) 197.
[2] E. Alves, A. Ramos, N. Barradas, F. Vaz, P. Cerqueira, L. Rebouta, U. Kreissig, Surf. Coat. Technol. 180–181 (2004) 372.
[3] F. Vaz, P. Cerqueira, L. Rebouta, S.M.C. Nascimento, E. Alves, Ph. Goudeau, J.P. Rivière, K. Pischow, J. de Rijk, Thin Solid Films 447–448 (2004) 449.
[4] F. Vaz, P. Carvalho, L. Cunha, L. Rebouta, C. Moura, E. Alves, A.R. Ramos, A. Cavaleiro, Ph. Goudeau, J.P. Rivière, Thin Solid Films 469–470 (2004) 11.
[5] E. Ariza, L.A. Rocha, F. Vaz, L. Cunha, S.C. Ferreira, P. Carvalho, L. Rebouta, E. Alves, Ph. Goudeau, J.P. Rivière, Thin Solid Films 469–470 (2004) 274.
[6] N. Martin, R. Sanjines, J. Takadoum, F. Levy, Surf. Coat. Technol. 142–144 (2001) 615.
[7] M. Bhat, L.K. Han, D. Wristers, J. Yan, D.L. Kwong, J. Fulford, Appl. Phys. Lett. 66 (1995) 1225.
[8] S.V. Hattangady, H. Niimi, G. Lucovsky, Appl. Phys. Lett. 66 (1995) 3495.
[9] W.L. Hill, E.M. Vogel, V. Misra, P.K. McLarty, J.J. Wortman, IEEE Trans. Electron. Devices 43 (1996) 15.
[10] P. Ponthiaux, F. Wenger, D. Dress, J.P. Celis, Wear 256 (2004) 459.
[11] S. Jemmely, D. Mischler, Tribol. Int. 32 (1999) 295.
[12] P. Jemmely, S. Mischler, D. Landolt, Wear 237 (2000) 63.
[13] F. Galliano, E. Galvanetto, S. Mischler, D. Landolt, Surf. Coat. Technol. (2001) 121.
[14] S. Mischler, A. Spiegel, M. Stemp, D. Landolt, Wear 251 (2001) 1295.
[15] S. Mischler, A. Spiegel, D. Landolt, Wear 225–229 (1999) 1087.
[16] D. Landolt, S. Mischler, M. Stemp, Electrochim. Acta 46 (2001) 3913.
[17] S. Barril, S. Mischler, D. Landolt, Tribol. Int. 34 (2001) 599.
[18] E. Ribeiro, A. Malczyk, S. Carvalho, L. Rebouta, J.V. Fernandez, E. Alves, A.S. Miranda, Surf. Coat. Technol. 151–152 (2002) 515.
[19] L.R. Doolittle, Nucl. Instrum. Methods B9 (1985) 344.
[20] M. Ohring, The Materials Science of Thin Films, Academic Press Inc., San Diego, 1992.
[21] J.A. Thornton, Am. Rev. Mater. Sci. 7 (1977) 239.
[22] R. Wuhrer, W. Yeung, M. Phillips, G. McCredie, Thin Solid Films 290–291 (1996) 339.
[23] C. Liu, A. Leyland, Q. Bi, A. Matthews, Surf. Coat. Technol. 141 (2001) 164.
[24] S. Mischler, P. Ponthiaux, Wear 248 (2001) 211.